Modeling of Aqueous Poly(oxyethylene) Solutions: 1. Atomistic Simulations

Jan Fischer,[†] Dietmar Paschek,[‡] Alfons Geiger,[‡] and Gabriele Sadowski*,[†]

Chair of Thermodynamics, Technische Universität Dortmund, Emil-Figge-Str. 70, 44227 Dortmund, Germany, and Chair of Physical Chemistry, Technische Universität Dortmund, Otto-Hahn-Str. 6, 44221 Dortmund, Germany

Received: August 14, 2007; In Final Form: December 4, 2007

The performance of different recently proposed force fields in combination with TIP4P-Ewald (TIP4P-Ew) water in reproducing experimental data of liquid 1,2-dimethoxyethane (DME) and its aqueous solutions for conformer populations, densities of solutions, and self-diffusion coefficients was explored. A modified version of the OPLS force field ("engineered") showed best performance in describing the conformer equilibria, but extremely high interconformational barriers reduce its applicability in dynamical simulations. The TraPPE-united atom force field (TraPPE-UA) by Siepmann et al. (*J. Phys. Chem. B* **2004**, *108*, 17596) was found to perform best in reproducing thermodynamic properties, but it showed some deficiency in describing the conformer equilibria. We reparameterized the dihedral potentials to match recent ab initio data by Anderson and Wilson (*Mol. Phys.* **2005**, *103*, 89) and could improve significantly the performance of description of conformer populations of DME in water. Subsequently, this modified TraPPE-UA was used in extensive simulations of poly(oxyethylene) oligomers $H(CH_2OCH_2)_nH$ (POE_n) with $n = 3$, 5, 10, 12, 20, 30 repeat units at mass fractions between 3% and 80% at 298 K. Density, radii of gyration, and diffusion coefficients are in very good agreement with available experimental data. We conclude that this force field in combination with the TIP4P-Ew water model is very suitable for simulations of poly(oxyethylene) oligomers in aqueous solution. The application to real polymeric systems on the atomistic level is however hindered by very slow decorrelation of large-scale features and by slow diffusion.

1. Introduction

Poly(oxyethylene) (POE) is an amphiphilic water-soluble polymer[1] showing complex phase behavior, including a closed-loop miscibility gap depending on molecular weight. It is used in a variety of application areas, e.g., protein crystallization[2,3] and purification, enhancing surface biocompatibility,[4] control of particle aggregation in solution,[5] and modification of membranes.[6] It shows very complex conformational behavior dependent on the polarity and nature of the solvent. A good force field should be able to describe the concentration dependency of these conformations as well as macroscopic thermodynamic equilibrium properties. POE has been studied previously by molecular simulations to gain insight into the thermodynamics and dynamics on an atomistic level.[7−12] Our aim in this paper is to critically evaluate different proposed force fields for their ability to describe aqueous POE solutions [CH_3-capped poly(ethylene glycol)]. We examine aqueous solutions of 1,2-dimethoxyethane (DME) as model compound, because it is the smallest species of the general formula $H(CH_2OCH_2)_nH$ containing all dihedral types present in the POE molecule. A good description of its conformational and other equilibrium properties should be a good indication of the quality of description to expect for the polymers of higher molecular weight. DME has already attracted much attention as model compound for POE.[10,13−16]

In the following, we first compare the performance of five different force fields in describing ab initio potential energies of different conformers. Then we discuss the quality of description of conformer populations in the bulk liquid and in aqueous solutions of dimethoxyethane and its thermodynamic and dynamic properties. We discuss two modifications of the OPLS-AA force field by Anderson and Wilson ("OPLS-engineered" and "OPLS-DMEFF"),[14] the Smith et al. force field,[13,17] and the TraPPE-UA force field by Siepmann et al.[18] Finally, we show that a modification of the dihedral potentials of the latter yields an accurate united atom-description of thermodynamics and structure of DME−water solutions.

2. Methods

2.1. Simulation Details. All simulations have been performed by employing the GROMACS 3.2.1 program[19,20] at 1 bar using a time step of 2 fs. After a short *NVT* equilibration period with total velocity rescaling, a 100−500 ps *NPT* equilibration was applied before data acquisition was started. We employed the Nosé-Hoover thermostat[21,22] with a relaxation time of 2.5 ps for the aqueous solutions and 1 ps for pure water simulations and a Rahman−Parrinello barostat[23,24] with relaxation time of 5 ps for aqueous solutions and 2.5 ps for pure water simulations. The compressibility of water at 300 K of 4.5×10^{-5} bar^{-1} was used for all simulations. Electrostatics were treated by employing the smooth particle mesh Ewald method[25] with a real space cutoff of 0.9 nm, a Fourier mesh spacing of 0.12 nm, and fourth-order interpolation. Lennard-Jones interactions were cut off at 0.9 nm with tail corrections for both potential and pressure. We used a Verlet-type neighbor list updated every 10 steps with a list cutoff radius of 0.9 nm. Constraints were solved using the SHAKE algorithm[26] with a relative iteration tolerance of 10^{-4}. Reported simulation results for density, radial distribution

* Corresponding author. Phone: +49-(231)-755-2635. Fax: +49-(231)-755-2075. E-mail: g.sadowski@bci.uni-dortmund.de.
[†] Chair of Thermodynamics.
[‡] Chair of Physical Chemistry.

10.1021/jp0765345 CCC: $40.75
Published on Web 02/06/2008

TABLE 1: Summary of Force Field Parameters Used for the Indicated Models, except for Torsions (see Table 2)[a]

	TraPPE-UA[18]			TraPPE-UA modified (this work)			OPLS-DMEFF[14]			OPLS-engineered[14]			Smith et al.[13,17]		
site	ϵ/k_B (K)	σ (Å)	q (e)	ϵ/k_B (K)	σ (Å)	q (e)	ϵ/k_B (K)	σ (Å)	q (e)	ϵ/k_B (K)	σ (Å)	q (e)	ϵ/k_B (K)	σ (Å)	q (e)
C(H3)	98	3.75	+0.25	98	3.75	+0.25	33.2	3.5	+0.11	33.2	3.5	+0.11	47.84	3.4477	−0.163
C(H2)	46	3.95	+0.25	46	3.95	+0.25	33.2	3.5	+0.14	33.2	3.5	+0.14	47.84	3.4477	−0.066
O	55	2.8	−0.5	55	2.8	−0.5	70.45	2.9	−0.4	70.45	2.9	−0.4	100.71	2.8509	−0.256
H	–	–	–	–	–	–	15.1	2.5	+0.03	15.1	2.5	+0.03	4.935	3.0025	+0.097

bonds	r_0 (Å)	k_{ij} [kJ/(mol Å^2)]	r_0 (Å)	k_{ij} kJ/(mol Å^2)]	r_0 (Å)	k_{ij} [kJ/(mol Å^2)]	r_0 (Å)	k_{ij} [kJ/(mol Å^2)]	r_0 (Å)	k_{ij} kJ/(mol Å^2)]
C−C	1.54	2177	1.54	2177	1.529	2244.1	1.529	2244.1	1.51	2587.44
C−O	1.41	2679	1.41	2679	1.41	2679.6	1.41	2679.6	1.39	3094.05
C−H	–	–	–	–	1.09	2847	1.09	2847	1.09	2742.35

bends	ϕ_0 (deg)	k [kJ/(mol rad^2)]	ϕ_0 (deg)	k [kJ/(mo l rad^2)]	ϕ_0 (deg)	k [kJ/(mol rad^2)]	ϕ_0 (deg)	k [kJ/(mol rad^2)]	ϕ_0 (deg)	k [kJ/(mol rad^2)]
C−C−O	112	418.2	112	418.2	109.5	418.68	109.5	418.68	109.04	720.13
C−O−C	112	519.6	112	519.6	109.5	501.22	109.5	501.22	111.56	623.83
H−C−H	–	–	–	–	107.8	275.7	107.8	275.7	108.3	322.39
H−CC	–	–	–	–	110.7	313.26	110.7	313.26	109.49	360.07
H−C−O	–	–	–	–	109.5	293.08	109.5	293.08	110.07	468.92

[a] Bond strengths for modified TraPPE taken from the OPLS-AA force field,[51] as TraPPE assumes rigid bonds. All parameters for harmonic bonds and angle bending interactions indicated are used as $u_{bond}(r) = {}^1/_2 k^{AB}(r - r_0{}^{AB})^2$ and $u_{bend}(\phi) = {}^1/_2 k_{ABC}(\phi_0{}^{ABC} - \phi)^2$.

TABLE 2: Summary of Force Field Parameters for Torsions[a]

		TraPPE-UA[18]		TraPPE-UA modified (this work)		OPLS-DMEFF[14]		OPLS-engineered[14]		Smith et al.[13,17]	
Dihedrals	n_i	k_i (kJ/mol)	$\phi_{0,I}$ (deg)	k_i (kJ/mol)	$\phi_{0,i}$ (deg)	k_i (kJ/mol)	$\phi_{0,i}$ (deg)	k_i (kJ/mol)	$\phi_{0,i}$ (deg)	k_I (kJ/mol)	$\phi_{0,i}$ (deg)
O−C−C−O	0	2.092 088	0	−7.759 67	0	–	–	–	–	−2.616 75	0
	1	–	–	7.585 26	0	5.902 966	0	1.558 5	0	−0.104 670	0
	2	−2.092 088	180	6.705 23	0	−5.360 362	180	−6.107 1	180	5.338 12	0
	3	8.368 265	0	8.400 71	0	1.719 941	0	5.847 9	0	–	–
	4	–	–	0.632 21	0	−1.926 556	180	9.399 2	180	–	–
	5	–	–	0.110 63	0	–	–	–	–	–	–
	6	–	–	0.359 62	0	–	–	–	–	–	–
	7	–	–	0.016 83	0	–	–	–	–	–	–
C−O−C−C	0	–	–	−0.253 90	0	–	–	–	–	−2.114 322	0
	1	6.030 902	0	−5.159 97	0	3.491 372	0	−3.271 4	0	2.093 384	0
	2	−1.361 495	180	−0.697 11	0	−1.183 398	180	4.758 7	180	1.465 367	0
	3	4.641 138	0	5.350 13	0	−0.006 909	0	6.414 4	0	0.669 901	0
	4	–	–	0.803 12	0	−0.613 575	180	−2.652 1	180	–	–
	5	–	–	0.283 07	0	–	–	–	–	–	–
	6	–	–	0.095 26	0	–	–	–	–	–	–
	7	–	–	−0.057 97	0	–	–	–	–	–	–
H−C−C−H	0	–	–	–	–	–	–	–	–	−0.293 076	0
	3	–	–	–	–	0.665 7	0	0.665 7	0	0.586 153	0
O−C−C−H	0	–	–	–	–	–	–	–	–	−0.293 076	0
	3	–	–	–	–	0.979 06	0	0.979 06	0	0.586 153	0
C−O−C−H	0	–	–	–	–	–	–	–	–	−0.847 827	0
	3					31.589 9	0	31.589 9	0	1.695 654	0

[a] All parameters are used according to $U_{dihed}(\phi) = \sum_{i=0}^{n} k_i[1 + \cos(n_i\phi - \phi_{0,i})]$. OPLS-AA and Smith et al. notation has been transformed using a phase shift of 180° if necessary.

functions, conformer populations, and self-diffusion were evaluated from production runs that lasted 2−10 ns in case of dimethoxyethane and its solutions and at least double the end-to-end vector autocorrelation time for longer oligomers. The TIP4P-Ew (TIP4P-Ewald) force field[27] for water was employed in combination with the respective force field for ether molecules (see Tables 1 and 2 for parameters). Simulation of oligomer solutions with $3 \leq n \leq 30$ were all performed using the TraPPE-UA with dihedral parameters modified in this work. Cross-parameters were determined applying the Lorentz−Berthelot mixing rules[28] for the TraPPE force fields and the OPLS-mixing rules[29] for the OPLS-based force fields, respectively. The results for the Smith et al. force field were taken from refs 30 and 31.

2.2. Force Field Performance and Modification. In order to evaluate the strengths and weaknesses of the different examined force fields with respect to the reproduction of structural and thermodynamic data, we used them in simulations of the dimer dimethoxyethane $H(CH_2OCH_2)_2H$ in aqueous solution and in the pure liquid. The thermodynamic properties in terms of the density (see Figure 5) are described best by the TraPPE-UA force field, which was fitted explicitly to reproduce thermodynamic properties (pure component densities and vapor pressures of several small ethers). It has been used before in simulations of poly(ethylene glycol) [or synonymously poly(ethylene oxide) dimethyl ether] in the melted state,[32] where it has been shown to reproduce both thermodynamic and structural

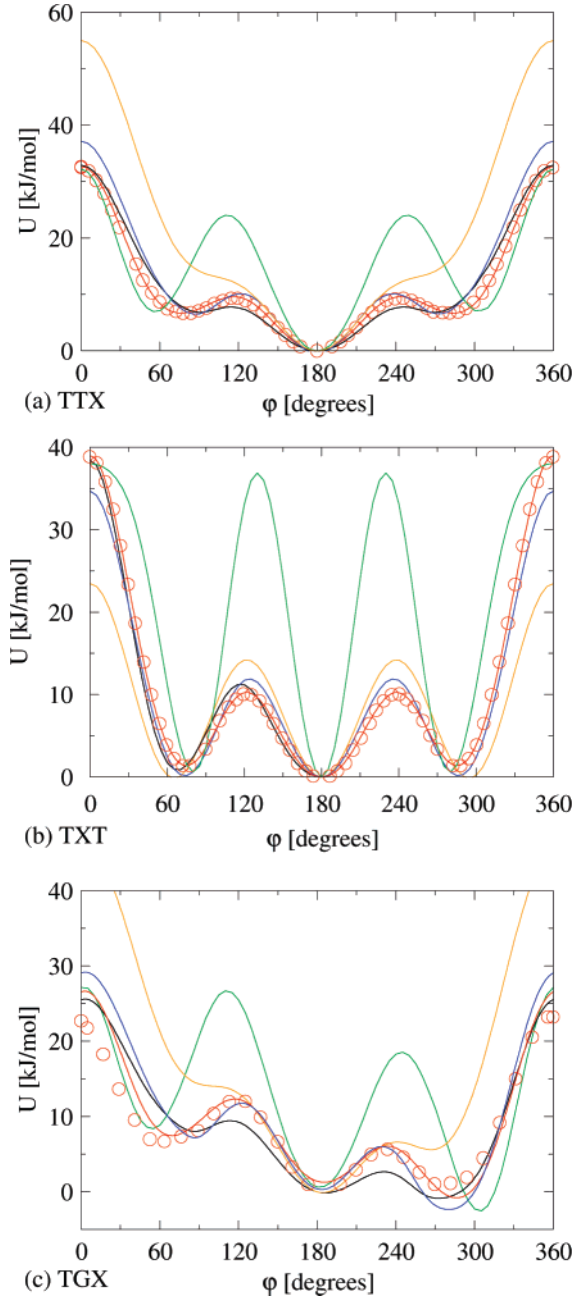

Figure 1. Potential energy of DME dependent on the conformations of the dihedrals C−C−O−C and O−C−C−O from ab initio calculations by Anderson and Wilson[14] (AI) (symbols) and from calculations using different force fields (lines): OPLS-DMEFF[14] (black), OPLS-engineered[14] (green), Smith[17] (blue), TraPPE-UA[18] (orange), and the modified TraPPE-united atoms force field from this work (red). (a) TTX: the first two dihedrals in trans conformation. The ab initio data were used to parametrize the new dihedral potential for C−O−C−C. (b) TXT: the two outer dihedrals in trans conformation. The ab initio data were used to parametrize the new dihedral potential for O−C−C−O. (b) TGX: the two outer dihedrals in trans−gauche conformation. All potential energies are relative to the conformer TTT.

data very well. However, our simulations revealed a significant mismatch of the conformer populations with experimental data, especially for this force field (compare Figures 3 and 4). The experimental conformer distributions (based on Raman measurements[33]) could not be reproduced very well by the TraPPE-UA force field. Both in the bulk liquid and in aqueous solutions, the original TraPPE-UA force field yields mainly TGT (T = trans, G = gauche) conformers (approximately 90%), while experiments show that, although TGT is the most important

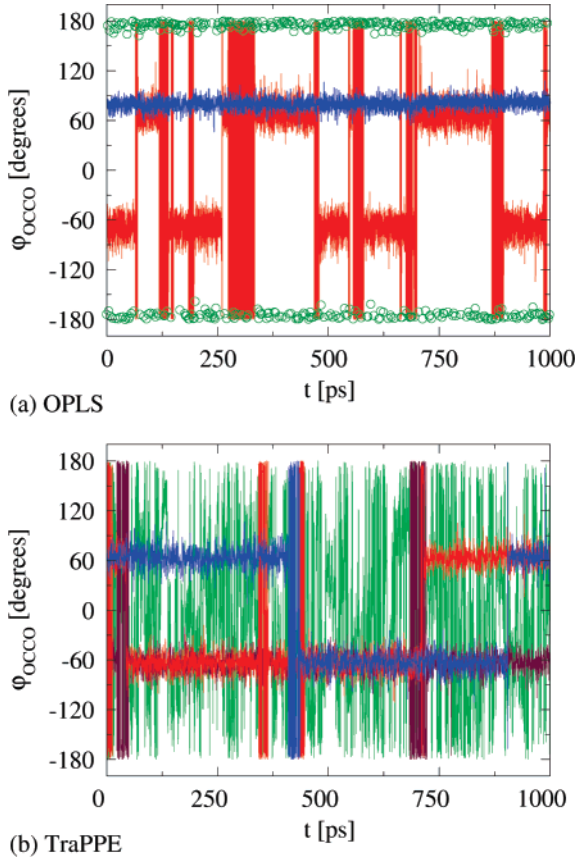

Figure 2. The state of the OCCO dihedral angle of one arbitrarily chosen DME molecule during 1 ns simulation of pure DME at 298 K using different force fields. (a) OPLS-force fields: red line, OPLS-DMEFF; blue line, OPLS-engineered, starting from a gauche conformation; green circles, OPLS-engineered, starting from a trans conformation. (b) TraPPE-UA and modified TraPPE-UA from this work: green line, TraPPE modified; red and blue line, TraPPE-UA.

conformer in aqueous solution and in the bulk liquid with populations of 40−60%, there are also significant populations of TGG′, TTT, and TGG. A detailed comparison of the conformer populations from molecular simulations with different force fields is given in the next section. We adopted the following assignment of conformations T, G, and G′ to the dihedrals: T refers to the range of angle 120°−240°, G to 0°−120°, and G′ to 240°−360°.

Reproduction of Ab Initio Data. In order to compare the performance of the different force fields in describing the relative potential energies of the different DME conformers correctly, we examined how well they could reproduce recent ab initio data by Anderson and Wilson.[14] They used the MP2/6-31G′++-(d,p) level of theory to determine relaxed potential energy surfaces for DME. Figure 1 shows the energies for (a) rotation around the outer carbon−oxygen bond (COCC), (b) rotation around the central carbon−carbon bond (OCCO), and (c) rotation around the outer carbon−oxygen bond with the two remaining dihedrals in trans conformation (a and b) and in trans−gauche conformation (c), respectively. The potential energy for the respective conformation relative to that of the all-trans conformation was determined for each force field by minimizing the molecule structure except for the angles that were kept fixed at 180° for trans and 75° for gauche (the latter corresponding to the gauche minimum angle of the ab initio OCCO energy; cf. Figure 1b).

The so-called "gauche effect" for the central OCCO dihedral, which has been the object of theoretical studies before,[10,16] is

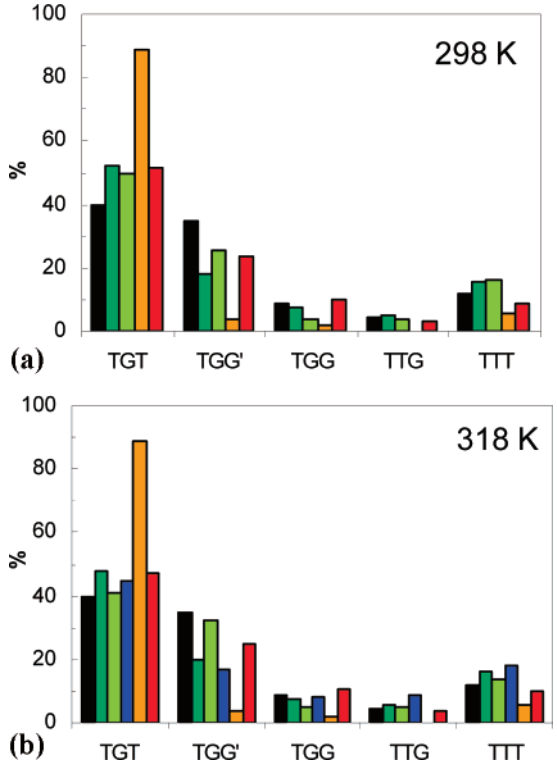

Figure 3. Distribution of the five most populated conformers of DME in the pure liquid phase at (a) 298 K and (b) 318 K. Results from Raman measurements[33] (black) and from molecular dynamics simulations with different force fields (from left to right): OPLS-DMEFF[14] (dark green), OPLS-engineered[14] (bright green), Smith[17] (blue), TraPPE-united atoms[18] (orange), and modified TraPPE-UA from this work (red).

obvious; i.e., the energy of the gauche conformations relative to the trans conformation is much lower than in the case of the COCC dihedrals; gauche conformations of the OCCO dihedral are thus energetically favored over trans conformations. Comparing the different force fields, it is obvious that the potential terms of the Smith et al. force field (LJ parameters from ref 17, other parameters from ref 13) yield a potential that is close to the ab initio data for OCCO and COCC dihedrals. The only notable deviation is a too narrow minimum for the COCC dihedrals being in gauche state (Figure 1a). The OPLS-DMEFF force field, which was fitted by Anderson and Wilson to reproduce their ab initio data, is very similar in that respect. It closely approximates the ab initio potential, but also exhibits a too narrow minimum for the gauche-state of OCCO and a too low barrier between trans and gauche states in the COCC dihedral. Their "engineered" force field shows some significant deviations, which is no surprise, because they refitted this force field with the aim of improving the description for the conformer populations in the bulk DME liquid. Specifically, they lowered the energy of the TGG′ conformer before fitting the OPLS-engineered dihedral parameters, thus making the TGG′ conformer the lowest energy conformer, which is not supported by their ab initio calculations. While this force field reproduces the absolute ab initio dihedral energy minima and locations for TTX and TXT (X = variable angle) conformations (see Figure 1), it shows great deviations in the peak maxima, and slight deviations in the location of the minima are present in comparison to the ab initio data. The noticeably lowered energy of the TGG′ conformer with respect to the ab initio result is obvious from Figure 1c.

Modified TraPPE-UA. The original TraPPE-UA force field shows some deficiency concerning the description of the gauche

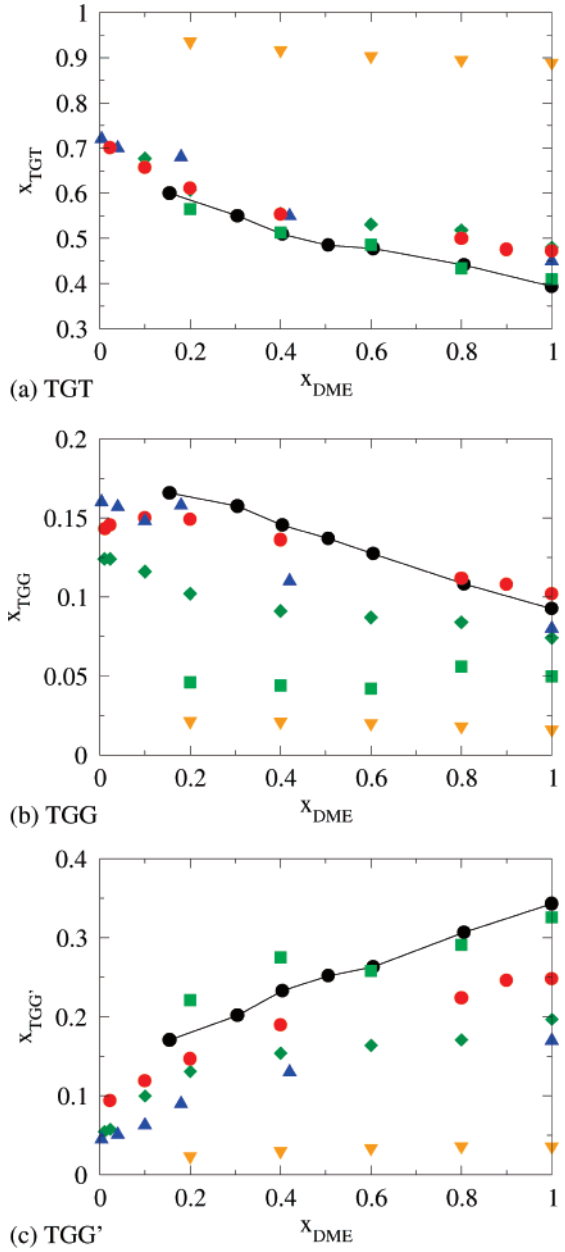

Figure 4. Population of the three most populated conformers of DME in aqueous solution at 318 K. Results from Raman measurements[33] (black circles and lines) and from molecular dynamics simulations employing the TIP4P-Ewald water model together with different force fields: OPLS-engineered[14] (green squares), OPLS-DMEFF[14] (dark green diamonds), Smith[17,35] (blue triangles up), TraPPE-UA[18] (orange triangles down), and modified TraPPE-united atoms (red circles) (this work). Conformers are (a) TGT, (b) TGG, (c) TGG′.

energies for the COCC dihedral. No pronounced minima for the gauche conformations are present in the curve for the TTX conformations (Figure 1). The TGX conformation energies are in turn not well reproduced either (Figure 1c), which leads to unfavorably high energy for the TGG′ conformer. The potential energy for the TXT and the corresponding gauche effect, on the other hand, is described qualitatively correctly (compare Figure 1). This leads to the large population of TGT conformers as described above. Gauche states are not favored for the COCC dihedrals, which results in very low populations of gauche states. Thus, there are far too low populations of the conformers TGG′ and TGG when using the TraPPE-UA force field. Hence, we chose to modify the TraPPE-force field to better reproduce the conformer populations. The original values of Siepmann et al.

for all parameters except dihedral interactions were retained (Table 1). The dihedral potentials for the groups C−O−C−C and O−C−C−O were refitted to the ab initio data shown in Figure 1a,b using a simple procedure: we switched off the dihedral angle potential along the respective four-connected atoms, but kept all other intramolecular interactions from bonded and nonbonded contributions switched on. The two remaining dihedral angles were fixed at 180°. Then we scanned through the angles and minimized the energy of the molecular structure with respect to all other degrees of freedom. Thus, we determined the angle-dependent (implicit torsional) potential that resulted only from *nondihedral* interactions. The dihedral potential to be parametrized is the difference between this "implicit torsional" potential and the ab initio potential. We used a proper dihedral potential of the form

$$U_{\text{dihed}}(\phi^{\text{ABCD}}) = \sum_{i=0}^{7} k_i[1 + \cos(n_i\,\phi^{\text{ABCD}} - \phi_{0,i}^{\text{ABCD}})] \quad (1)$$

to fit the two dihedral potentials for ABCD = O−C−C−O and C−O−C−C, respectively (parameters are shown in Table 2 along with the dihedral parameters of the other force fields). The phase angle $\phi_{0,i}^{\text{ABCD}}$ has been taken to be 0 for all terms. The potential energies of TTX and TXT conformations (X = variable angle) are described extremely well with this parametrization (compare Figure 1, parts a and b) and the TGX conformation energies are described better than by all other examined force fields (Figure 1c). The potential minima of the TGX conformations take similar values for all force fields except for the OPLS-engineered and our modified force field. Consequently, the relative stabilities or sequence of energies of the different conformers in vacuo are the same for all force fields except for these two, where the TGG′ conformer is marginally more stable than the TTT conformer. Ab initio calculations in general suggest that the TTT conformer is the most stable, followed by TGT and then TGG′. However, there are, as shortly discussed by Anderson and Wilson, basis sets that lead to lower energy for the TGG′ conformer than for the TTT.[14] Our modification dramatically improves the description of the conformer equilibria in both bulk liquid and aqueous solution of DME by the TraPPE-UA force field, which now performs similarly well as the OPLS-engineered force field. The reparameterization leads to a small decrease in the TGG′ conformer energy without increasing significantly any inter-conformational barriers.

3. Results and Discussion

3.1. Force Field Performance for 1,2-Dimethoxyethane. Equilibration of Dihedrals. Simulations using the OPLS-engineered force field resulted in severe equilibration difficulties, with conformer populations depending heavily on the starting conformations. To examine if the large interconformational barriers for flipping the OCCO dihedral (Figure 1b) were the origin of this slowing down of equilibration, time series of individual dihedral angles OCCO were compared for the different force fields. Figure 2 shows the angle of the OCCO dihedral of one individual DME molecule from 1 ns simulation of pure DME at 298 K using different force fields.

The actual angle of each dihedral was sampled after every 0.2 ps. As expected from the high interconformational barriers, the OPLS-engineered force field shows extremely low flip rates of only 0.012 and 1.25 flips per molecule and per nanosecond for the OCCO and COCC dihedrals, respectively, in the pure liquid phase. It is obvious from Figure 2 that the dihedrals of individual molecules are trapped in their initial state for very long times when using this force field. The flipping of the OCCO dihedrals is such a rare event that simulations starting from a crystal-like all-trans conformation structure did in general not yield more than 5−10% of the OCCO dihedrals in the gauche-state, even after 6 ns. The OPLS-DMEFF force field shows quite frequent flipping of the OCCO dihedrals of approximately 69 flips/ns per molecule on average in the neat liquid phase. The COCC dihedrals flip even more often, approximately 540/ns in the pure liquid. The modified TraPPE-UA shows comparably frequent flipping of the dihedrals as the OPLS-DMEFF force field in the pure liquid phase of approximately 55 flips/ns and 236 flips/ns for the OCCO/COCC dihedrals, repectively. Both rates are increased compared to the original TraPPE-UA (OCCO, 7.3 flips/ns; COCC, 123 flips/ns). We would expect a still more frequent flipping compared to the all-atom models. The observation that the flipping is at a similar rate could perhaps be explained by the fact that two opposite effects nearly cancel out: reduced steric resistance for the united atom model favors a higher flipping rate, but the stronger electrostatic interactions that occur because of the higher partial charges in the TraPPE-UA model than in the AA models slow down the flipping.

In aqueous solution, the OCCO flip rate is reduced, except for the engineered OPLS. We observed 15−26 flips per nanosecond and molecule with the OPLS-DMEFF for x_{DME} = 0.1−0.2. This is in good agreement with results by its authors,[34] who used their force field in simulations of an isolated POE_{16} chain and of four amphiphilic polymer molecules having a POE_{15} side chain, both in TIP4P-water. They noted rates of 25 flips/ns for the terminal OCCO dihedral of the side chains and 6 flips/ns for the terminal of the isolated POE_{16} chain. Their reported flip rate for the COCC dihedral is much lower than ours. The rate at which the OCCO dihedrals undergo changes is comparable for all force fields (Smith et al. reported approximately 50 flips/ns for DME simulations)[35] except for the OPLS-engineered.

When comparing the conformer populations that result from simulations starting either from a crystal-like all-trans configuration or a thoroughly equilibrated configuration (using OPLS-DMEFF) as starting point, we observe that the results of Anderson and Wilson for the bulk DME conformer populations (seemingly at 300 K; see Table 3 in their paper) can only be reproduced in the latter case. Only in that case could the published populations[14] of the three main conformers of pure DME be reproduced within 2% at 298 K. Here, our simulations yielded slightly more TTT and TGT conformers and slightly less TGG′. Using the all-trans configuration, most of the central OCCO dihedrals essentially remained in their starting state, yielding only negligible amounts of the experimentally most important TGT and TGG′ conformers. We conclude that OPLS-engineered seems to be not very appropriate for molecular dynamics simulations, because it needs very long equilibration times or previous equilibration by different means.

Conformational Equilibria in the Bulk Liquid. Figure 3 shows populations of the five main conformers of 1,2-dimethoxyethane in the pure liquid at 298 and 318 K. We compare Raman measurement results and simulations using the different force fields. The TGT population is overestimated by all force fields to different extents, while the second-most important conformer population of TGG′ is underestimated. Immediately evident is the deficiency of the original TraPPE-UA in describing the conformer equilibrium, which led to our proposed dihedral potential modification. This modification

improves the description such that the accordance with experiment at 298 and 318 K is now comparable to that of the OPLS-DMEF force field and better than that of the force field by Smith et al. for TTT, TGG, and TGG′ in the bulk liquid at 318 K (no data given by Smith et al. for 298 K). The deviation from experiment for the two most populated conformers is smallest when using the OPLS-engineered force field at 318 K. At 298 K, our modified force field performs comparably well. Taking into account the practical impossibility of equilibration using only the OPLS-engineered force field (see previous section), this performance advantage is questionable. As we are want to carry out simulations of aqueous POE solutions, improving the representation of the conformational equilibria in aqueous solution is more important to us.

Conformer Populations in Aqueous DME Solutions. Figure 4 shows results for conformational populations in aqueous solutions at 318 K from simulations and experiments. Water was represented by the TIP4P-Ewald model, except for the Smith et al. force field, where results form simulations with TIP4P-water have been taken from refs 30 and 35. The dependency on concentration of TGT and TGG′ populations as measured by Goutev et al.[33] is generally captured correctly by all examined force fields. The increasing population of the TGG conformer when approaching more diluted solutions is not described by the engineered force field, where the population of this conformer is nearly concentration-independent. The deviation between simulation and experiment for the most frequent conformer TGT is comparable for all force fields. The Smith et al. and OPLS-DMEFF force fields overestimate its fraction, while our modified TraPPE-UA underestimates it to the same extent. The Anderson and Wilson engineered force field performs best, but only after a lengthy equilibration with different means. The population of the second-most populated conformer TGG′ is also described best by this force field. The scatter in the data is generally highest with this force field, probably again originating from the low dihedral flip rates. The values at midconcentrated state points, where water and DME interact most strongly (maximum of the excess volume is at about $x_{DME} = 0.4$), seem not yet to be at equilibrium. Second-best for the TGG′ is the modified TraPPE-UA followed by the OPLS-DMEFF and the Smith et al. force field. The TGG conformer population is reproduced best by our modified TraPPE-force field. Its population seems to reach a maximum at around 10% DME and is reduces for lower concentrations with the modified TraPPE. A saturation plateau at low concentrations can be observed with the OPLS-DMEFF force field and the Smith force field. The OPLS-engineered force field underestimates the TGG population by approximately 50% and cannot describe the concentration-dependency at all. Summing up, our modified TraPPE-UA performs best of the examined force fields in describing the temperature and concentration dependency of the main DME conformers in dynamical simulations.

Comparison with Volumetric Data. Both the original TraPPE-UA and the modified TraPPE-UA force field show excellent agreement with the experimental data for the density of aqueous dimethoxyethane solutions when combined with the TIP4P-Ewald water model, using the simple Lorentz−Berthelot mixing rules (Figure 5). The performance is considerably better than for the OPLS-based force fields and comparable to the Smith force field (data taken from ref 31; we did not try to reproduce their data, because the employed force field parameters they used are not clearly indicated). For high concentrations of 80% and more DME, the agreement between experimental and simulated densities is better for the original TraPPE-UA than for all other force fields. In the diluted to midconcentrated region, the modified TraPPE performs best. Within the mid-concentrated region to the pure liquid DME, the dihedral modification shows greater deviations from experimental density, leading to an underestimation by about 2%. Here, TraPPE-modified force field performs similarly well as the OPLS force fields. We also tested the performance of the modified TraPPE-UA force field in reproducing the density of aqueous di- and tetraethylene glycol dimethyl ether ($[H_3C(OCH_2CH_2)_nOCH_3$, $n = 2, 4]$ solutions (Figure 8). We found excellent accordance with experiments, including a quantitative description of the excess density, which takes positive values for small concentrations, reverses to negative values for diglyme at about $x_{POE_3} \approx 0.3$, and is positive over the whole concentration range for tetraglyme. The OPLS-DMEFF force field fails in describing this tendency even qualitatively and shows a negative excess density at small concentrations. The quality of description of aqueous mixtures relies very much on the water model used. TraPPE-UA has recently been used for aqueous tri- and tetra-(ethylene glycol) solutions $[H(OCH_2CH_2O)_nH$, $n = 3, 4]$ in combination with the modified SPC/E water model.[36] The mixture density was systematically underestimated by 3−7% compared to experimental data.[37] From our observations, we conclude that the TIP4P-Ew model, which has been shown to yield a very accurate description of pure water properties,[27,36,38] can successfully be used to describe properties of aqueous POE solutions as well.

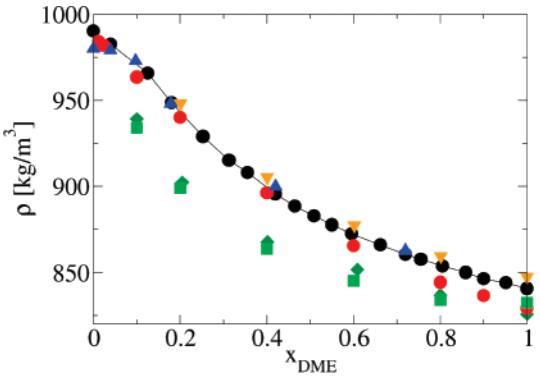

Figure 5. Density of aqueous DME solutions at 318 K. Comparison between experiments[52] (black circles and line) and results from molecular dynamics simulations with TIP4P-Ewald water and different force fields: OPLS-DMEFF[14] (green diamonds), OPLS-engineered[14] (bright green squares), Smith (simulation results with TIP4P-water from ref 31) (blue triangles up), TraPPE-united atoms[18](orange triangles down), and modified TraPPE-UA from this work (red circles).

Radial Distribution Functions. We compared the radial distribution between water oxygens and DME oxygens at different concentrations (Figure 6). The structuring of water around the ether oxygens increases with increasing DME concentrations, visible in the increasing first peak of the $g(r)$. There is little difference among the TraPPE force fields on the one hand and among the OPLS-based force fields on the other hand. The local water oxygen density is greatly reduced in the OPLS simulations compared to the bulk for concentrations up to 60% DME, showing a less favorable hydration of the ether oxygens, which may indicate a tendency to demix. The TraPPE radial distribution functions, on the other hand, resemble more the pure water $g(r)$ and show a good reciprocal miscibility of DME and water. This could explain the consistently too low density of aqueous DME solutions with OPLS (approximately 5%, compare Figure 5). The even greater disagreement between experimental density and simulation for the diethylene glycol

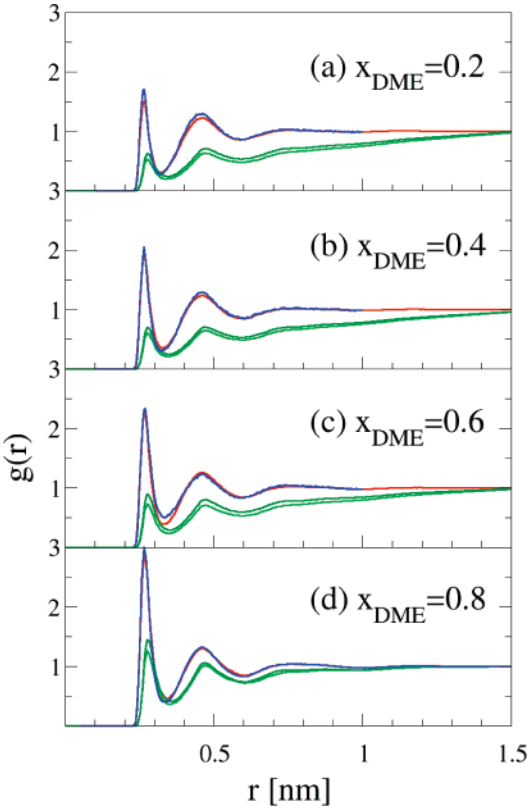

Figure 6. Radial distribution function between ether oxygens and water oxygens at 298 K from simulations of aqueous DME solutions using TIP4P-Ewald water with OPLS-DMEFF[14](dark green), OPLS-engineered[14] (bright green), TraPPE-UA (red line), and modified TraPPE-UA (blue line) (this work). (a) $x_{DME} = 0.2$; (b) $x_{DME} = 0.4$; (c) $x_{DME} = 0.6$; (d) $x_{DME} = 0.8$.

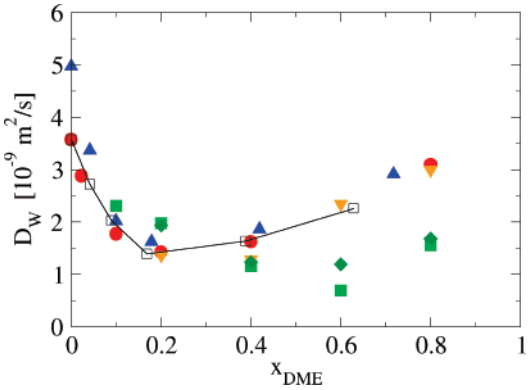

Figure 7. Concentration-dependence of the water self-diffusion coefficient in aqueous solutions of DME at 318 K from experiments[31,39] (open squares and line) and from MD simulations employing the TIP4P-Ewald water model in combination with the force fields OPLS-DMEFF[14](green diamonds), OPLS-engineered[14] (bright green squares), TraPPE-UA[18] (orange triangles down), and modified TraPPE-UA force field from this work (red circles). Blue triangles up: simulation results by Bedrov et al. using the Smith et al. force field with TIP4P-water.[31] The experimental data have been scaled to reproduce the pure water self-diffusion coefficient at 318 K reported by Mills[39] and Holz et al.[42]

dimethyl ether solutions (Figure 8) using the OPLS-DMEFF force field could also originate from this local demixing. The favorable interactions between water and DME in terms of DME hydration are weaker in the OPLS simulations than those in the TraPPE simulations, thus making the overall solution structure less compact and the density too low. The interactions among DME-molecules, on the other hand, are more favorable in the OPLS than in the TraPPE-description, resulting in higher

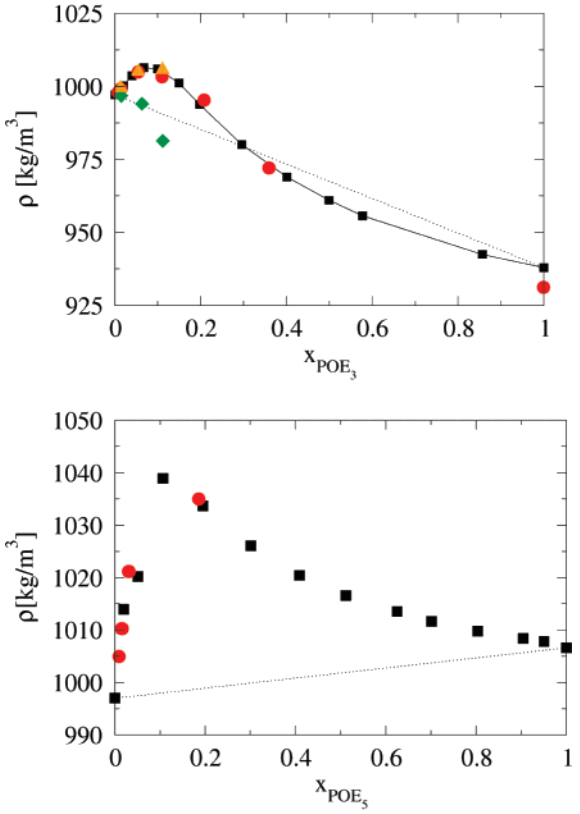

Figure 8. Density of aqueous POE_3 (diglyme, diethylene glycol dimethyl ether) and POE_5 (tetraglyme, tetraethylene glycol dimethyl ether) solutions at 298 K. Comparison between experiments[53,54] (black squares and full line) and results from molecular dynamics simulations with TIP4P-Ewald water and (a) the OPLS-DMEFF[14] force field (green diamonds), (b) the TraPPE-UA force field[18] (orange triangles), and (c) with the modified TraPPE force field (red circles) from this work. The broken line shows the ideal mixture density.

peaks for the ether oxygen−oxygen radial distribution function than for the ether oxygen−water oxygen radial distribution function (not shown). The pure DME oxygen-radial distribution function is very similar for all force fields (not shown).

Self-Diffusion. Figure 7 shows water self-diffusion coefficients in aqueous DME solution at 318 K from simulations together with experimental data by Bedrov et al.[31] The mean squared displacement (MSD) of molecules from the center of mass motion was evaluated according to

$$\mathrm{MSD}(\delta t) = \langle |\vec{r}_{\mathrm{com},i}(t+\delta t) - \vec{r}_{\mathrm{com},i}(t)| \rangle_{t,i} \qquad (2)$$

Here, the brackets denote averaging over both many time origins and all molecules of interest. Using the Einstein relation, the self-diffusion coefficient can be calculated from the long-time linear slope as

$$D_{\mathrm{self}} = \frac{1}{6} \lim_{\delta t \to \infty} \frac{\partial}{\partial \delta t} MSD(\delta t) \qquad (3)$$

As the original published value for the pure water self-diffusion coefficient by Bedrov et al. seemed to be unrealistically high when compared with a wealth of available diffusivity data published,[39−42] their data was scaled such that the experimental value of approximately 3.6×10^{-9} m^2/s at 318 K was reproduced. This value was determined by Mills[39] using a diaphragm-cell technique and independently confirmed by recent pulsed magnetic field gradient NMR measurements by Holz et al.[42] All force fields are able to describe the concentration dependency of the water self-diffusion coefficient qualitatively.

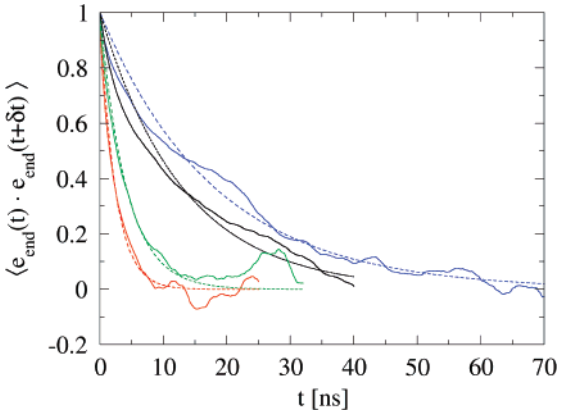

Figure 9. Orientational autocorrelation function of unit vectors parallel to the vectors connecting the chain ends from atomistic simulations of POE in water for different polymer chain lengths at monomer concentration 0.27 (force fields: TraPPE-UA, modified in this work, and TIP4P-Ew). Full lines denote results from simulation, broken lines are exponential fits of the curves. Number of monomers are 10 (red), 12 (green), 20 (black), and 30 (blue).

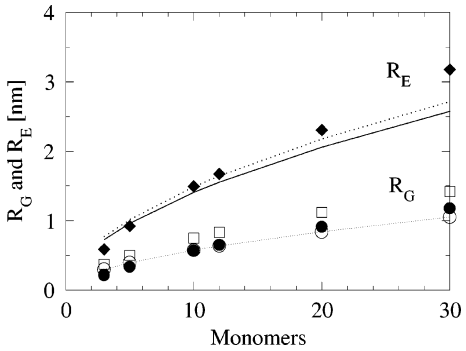

Figure 10. Radius of gyration R_G (circles) and end-to-end distance R_E (diamonds) for POE oligomers in water at 298 K and 1 bar: full symbols, atomistic simulations at constant segment concentration $x_{PEO} = 0.27$ in TIP4P-Ewald water; open symbols, values calculated by extrapolation of experimental data of longer chains from Kawaguchi et al.[45] (circles) and Devanand et al.[46] (squares). The full line shows R_E values for an ideal chain having the experimental R_G value and the dotted line shows the same for an expanded chain.

The experimentally determined minimum at $x \approx 0.2$ is located at too high concentrations for the OPLS-based force fields ($x \approx 0.6$), and a considerable deviation from experiment is visible for concentrations higher than 0.4. The TraPPE-UA force field and its modified version reproduce the location and absolute value of the minimum very well and show the smallest deviations over the entire concentration range. The TIP4P-Ewald water model reproduces the pure water value nearly perfectly. According to Bedrov et al., different water models yield values between approximately 3.5×10^{-9} and 5.5×10^{-9} m^2/s (from ref 31), being either closer to the smaller experimental value that we consider more reliable (MCY, TIP4P-Ew) or closer to the higher value (TIP4P, SPC/E).[31] Bedrov et al. reported an experimental self-diffusion coefficient for neat DME liquid of 3.2×10^{-9} m^2/s at 298 K, which is in excellent agreement with the value from simulations with the modified TraPPE force field of 3.21×10^{-9} m^2/s (original TraPPE-UA, 3.16×10^{-9} m^2/s) (cf. Figure 11). The Smith et al. force field and the OPLS force fields yield too low values for pure DME of 2.3×10^{-9} and 2.01×10^{-9} m^2/s, repectively. Both models thus underestimate the DME mobility in the neat liquid. The self-diffusion coefficient of neat DME is well reproduced by both TraPPE force fields. To sum up, the quality of description of diffusion

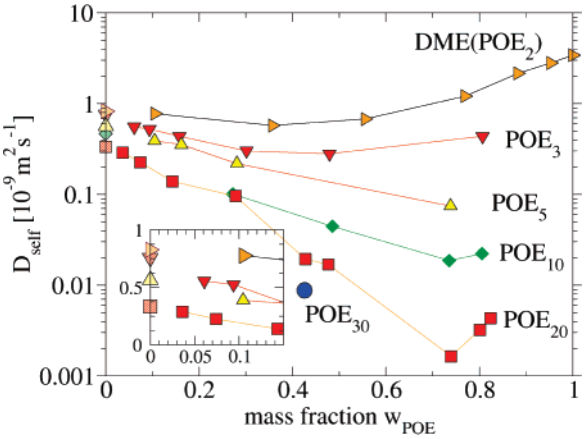

Figure 11. Self-diffusion coefficients of POE_n oligomers in aqueous solution with $n = 2, 3, 5, 10, 20, 30$ monomers from atomistic simulation at 298 K (TraPPE-UA modified and TIP4P-Ew) compared to experiments. Data points on the ordinate axis from experiments for poly(ethylene glycol) at infinite dilution from ref 50 (no. of monomers 2, 3, 5, 8, 21). The inset shows a magnification of the diluted region with the same key to the symbols.

for both pure components is best if using the TraPPE force fields with TIP4P-Ew and yields a similarly good description in the mixture.

3.2. Simulations of Aqueous POE Oligomer Solutions. Employing the modified TraPPE-UA force field and TIP4P-Ewald water, we simulated aqueous solutions of larger POE homologues $H(CH_2OCH_2)_nH$ (POE_n) with $n = 3, 5, 10, 12, 20, 30$ repeat units at 298 K and 1 bar. First, the polymer structures were built by assigning molecules in all-trans configuration onto a regular cubic lattice. Then these structures were solved in an appropriately sized box filled with a shortly equilibrated water configuration. Overlapping water molecules were deleted and concentration was adjusted by deleting further water molecules. The simulations were started at a greatly reduced density and allowed to equilibrate in two steps: first at constant volume with total temperature rescaling in every step employing the Berendsen thermostat. Then the system was allowed to move toward its equilibrium density during some 100 ps of NPT simulation (Nosé−Hoover thermostat and Rahman−Parinello barostat). Equilibrated box sizes ranged from 2.5 to 6.5 nm depending on concentration. All simulations included at least eight POE molecules (except the 30-mer with six molecules) and the total number of molecules in the simulation ranged from 290 to 1600. Reported results were calculated from sampling of at least 10 ns *NPT* simulation time with recording of configuration and thermodynamic data after every 100 steps. In cases where the autocorrelation time of the vectors connecting the polymer chain ends was significantly greater, simulations were continued to at least double the autocorrelation time, so that total simulation time reached 150 ns for the 30-mer. Averages were calculated from the simulation trajectories after the complete decay of the R_E-autocorrelation functions (compare Figure 9). These simulations served as additional validation of the modified atomistic force field and to generate atomistic reference data for mesoscale potential generation in the second part of this publication. We conducted simulations at a wide range of concentrations for all chain lengths except for the 30-mer.

Relaxation Behavior. To show that a thorough sampling of configuration space had taken place in all simulations, we calculated the autocorrelation function of the end-to-end vectors. This is a useful measure for longer chain molecules, because it

is one of the slowest modes observed within simulation. It is defined as

$$P(\delta t) = \langle \vec{e}_{\text{end}}(t)\, \vec{e}_{\text{end}}(t + \delta t) \rangle_{i,t} \tag{4}$$

where $\vec{e}_{\text{end}}(t)$ is the vector connecting the first and last monomer of the polymer chain at time t. The product is averaged over all molecules and many time origins of the trajectory. The functions evaluated from simulations (Figure 9) could be fitted by a simple monoexponential decay function given by

$$P(t) = \exp(-t/\tau_{\text{end}}) \tag{5}$$

τ_{end} denotes the autocorrelation time. The plot shows the autocorrelation functions according to eq 4 for the atomistic simulations having a monomer concentration of 0.27 [$x_{\text{mono}} = n_{\text{mono}}/(n_{\text{mono}} + n_{\text{water}})$]. Complete decorrelation is achieved for all simulated chain lengths. It increases drastically from 2.39 ns for POE_{10} and 6.7 ns for POE_{20} to 18.05 ns for POE_{30}. The 12-mer value is in quantitative agreement with results from Smith et al. using their force field.[8] POE_{30} gets totally decorrelated only after approximately 70 ns of simulation compared with approximately 10 ns for POE_{10} (compare Figure 9). For chains of 10 and more monomers, the autocorrelation times from the fit increase approximately as $N^{1.8}$, which is consistent with the theoretical behavior of a polymer in a good solvent.[43,44] All atomistic simulations were extended to times at least double the respective autocorrelation time. Our results show that in this case simulations of POE solutions with a degree of polymerization of significantly larger than 30 (corresponding to a molecular weight of 1323 g/mol) is rather impractical within acceptable computer time (total CPU time for 150 ns on an AMD Opteron 2.4 GHz processor: 862.5 h; 2996 atomic sites), even more so given the fact that we simulated a small molar concentration of $x = 0.01$ (corresponding, however, to a mass fraction of 0.426). This underlines the need for a coarser representation of the system if polymers of higher molecular weights are to be simulated.

Chain Dimensions. Two static properties, namely, the average radius of gyration and the average end-to-end distances, were evaluated from simulation. The radius of gyration (R_G) and end-to-end distance (R_E) are defined as

$$R_G = \sqrt{\left\langle \frac{\sum_i m_i |\vec{r}_i - \vec{r}_{\text{com}}|^2}{\sum_i m_i} \right\rangle} \tag{6}$$

$$R_E = \langle |\vec{r}_1 - \vec{r}_n| \rangle \tag{7}$$

where $\vec{r}_{\text{com}}$ denotes the center of mass of the molecule, $\vec{r}_i$ the position of site i, and m_i its mass, and $\vec{r}_1$ and $\vec{r}_n$ denote the position of the first and last atom of the chain, respectively. The averaging is performed over all molecules and equidistant snapshots from simulation (typically we recorded data after every 100 time steps, and the total number of data evaluated per concentration ranged from 10^4 to 10^6). Figure 10 presents radii of gyration from the atomistic simulations (3−30 monomers) along with extrapolated experimental data measured for considerably greater molecular masses (6×10^3 to 10^6 g/mol).[45,46] The accordance is very good, indicating that the modified TraPPE-force field is indeed capable of reproducing the essential static properties of longer-chain POE−water systems very well. Deviation between simulation and extrapolated data is only 1% for the decamer of molecular weight 442.3 g/mol and within 15% for greater monomer numbers. Comparing with extrapolated R_G measurements by Devanand and Selser[46] gives larger deviations, which is probably due to a greater error in extrapolation, as they measured POE at much higher molecular weights (>25 000 g/mol). The end-to-end distances from atomistic simulations are larger than the values one would expect for an ideal chain ($R_E = \sqrt{6} R_G$). We find $R_E^2/R_G^2 \approx 6.8$ for chains of 10−30 monomers, which is close to the theoretical value of 6.66 for expanded chains[44] (also plotted in Figure 10) and which can be explained by the more extended conformations that POE has in the good solvent water due to favorable hydration interaction. The error estimates based on the block average method by Flyvbjerg and Petersen[47] for 10 or more monomers range from 0.005 to 0.02 nm for R_G and 0.005 to 0.15 nm for R_E. The higher and smaller numbers correspond to the longest molecule at the smallest concentration and the smallest molecule at the highest simulated concentration, respectively. Errors are within these ranges for all concentrations and molecules of 10 and more monomers and below 0.005 nm for the trimer and pentamer. The scaling exponent we find for the gyration radius from least-squares regression of the atomistic simulations of oligomer chains is approximately 0.752. Thus, the oligomers show more stiffness than expected from long-chain scaling behavior. This is consistent with polymer theory, where scaling laws only apply in the limit of infinitely long chains. Reith et al. found a similar behavior for poly(acrylic acid) in water. Their simulations showed a scaling of R_G for small oligomers chains of approximately 0.8, while good agreement with theoretical long-chain behavior was found for chains of 100 monomers and more from their mesoscale simulations.[48] The 12-mer radius of gyration of 6.25 Å from our atomistic simulation at 298 K also agrees well with the value of approximately 7 Å reported by Smith et al. for 318 K for their atomistic simulations, considering that the chains show a moderate tendency in solution to extend more at higher temperature (the contrary is true in the melt).[49]

Self-Diffusion Coefficients. Figure 11 shows self-diffusion coefficients at varying mass fractions of DME and POE evaluated from MD simulations. On the ordinate axis, we show experimental data from PFG-NMR measurements[50] for self-diffusion coefficients at infinite dilution for poly(ethylene glycol) oligomers with $n = 3, 5, 8, 21$ monomers for comparison (same key to symbols as for the simulated values). A pronounced concentration dependency of the diffusion coefficients is evident. A considerable slowing down of diffusive motion for increasing concentrations can be seen for all chain lengths. This effect increases with chain length and yields concentration-dependent diffusion coefficients extending over several orders of magnitude for the longer chains. It reaches a minimum value at mid to high concentrations and increases again toward the pure melt. Two mechanisms can be considered for explanation: In the diluted region, viscosity is low, and contacts between chains are scarce. All chains are fully hydrated, but the hydration shells do not interfere. Upon concentrating the solutions, more contacts and overlaps between the polymer coils occur and lead to an increase in viscosity and in turn to a decrease of diffusional motion. At the same time, the hydrogen-bonding network between ether and water oxygens starts to slow down diffusion. Water can act as "glue" that bridges several ether oxygens via different structures involving one or more molecules, as POE fits quasiperfectly into the bulk water structure.[7,9] In the more concentrated region, there is not enough water to hydrate all chains; hence, the number of hydrogen-bonded ethers decreases,

as no hydrogen bonds can be formed among the ether oxygens alone. Overall, interactions are weaker and therefore diffusion increases again. The minimum concentration is found at around $w \approx 0.75-0.8$ for the 10/20-mer (as for POE_{12} in ref 8), while trimer and dimer show a minimum at around $w \approx 0.5$, which corresponds to the concentration where hydration is saturated.[7] The shift of the minimum toward higher concentrations for longer chains could be explained by the tendency of water to form multiple hydrogen bonds.[7] As simulations were performed at higher concentrations than used for the measurements in ref 50, extrapolation to infinite dilution is needed for comparison with experiment. Inspection of the diluted region $w < 0.15$ (inset in Figure 11) reveals that the experimental data fit well into the simulated data sets for 3-, 5-, and 20-mer. The most diluted 20-mer value from a single chain simulation at 3.4 mass-% compares very favorably with the experimental data (see inset in Figure 11). There is, however, a greater uncertainty in the coefficients at smaller concentrations, because the linear diffusion regime sets in rather slowly in the simulations of dilute systems. Overall, we conclude that the modified TraPPE-UA force field also captures the dynamics of longer oligomers rather nicely, as already shown for the dimer (Figure 7).

4. Conclusion

Five ether force fields were evaluated together with TIP4P-Ew water for their performance in simulations of the POE dimer 1,2-dimethoxyethane. One of these is the TraPPE-UA, which we combined with modified dihedral potentials. This force field represents the both concentration- and temperature-dependent conformer populations better than the original TraPPE-UA force field, the OPLS-DMEFF force field, and the Smith et al. force fields. We showed that our dihedral potential modification keeps the advantages of TraPPE-UA in terms of a nearly quantitative description of densities of aqueous solutions of POE oligomers like dimethoxyethane, diethylene glycol dimethyl ether, and tetraethylene glycol dimethyl ether, while the OPLS-based force fields fail to describe the mixture densities correctly. The OPLS-engineered force field shows good agreement for the conformer populations, but it has very high interconformational barriers for the OCCO dihedral and the density is not reproduced very well. We found that its slow dihedral orientational dynamics are of great disadvantage in molecular simulation, as equilibration is slowed down drastically; this is especially important for molecules with a great number of dihedrals like polymers. The Smith et al. force field performs well in terms of thermodynamics and conformer equilibria, as demonstrated by their authors in numerous papers. However, a disadvantage is that it uses a combination of Lennard-Jones and Buckingham terms and a special hydrogen-bonding term, the exact use of which is not always stated in the publications. The reproduction of their results with standard molecular simulation programs is thus hindered. The TraPPE-based modified force field only uses common functional force field terms and has the computational advantage of being a united atom model. Self-diffusion of both water and dimethoxyethane are described best by the TraPPE force fields and second-best by the models of Smith et al. We further showed in extensive simulations of POE oligomers $H(CH_2OCH_2)_nH$ with up to 30 monomers that the TraPPE-UA force field together with TIP4P-Ew is able to capture many thermodynamic as well as dynamic and structural properties of aqueous solutions of these large oligomers on the atomistically detailed level of description very well. However, examination of relaxation functions reveals that in order to simulate real polymeric molecules with hundreds of monomers, the models have to be considerably coarser. Departing from atomistic reference data generated in this work, we will develop a coarse-grained description of POE solutions in the second part of this series of publications. As the accuracy of mesoscale potentials relies on the accuracy of the underlying atomistic force field, we can be confident that the coarse-grained potentials derived hereafter will also incorporate the essential properties of the polymer solutions under examination.

Acknowledgment. The authors are grateful to Deutsche Forschungsgemeinschaft (DFG) and to the Technische Universität Dortmund for kindly providing computer time on its Linux Cluster Dortmund (LIDO).

References and Notes

(1) Bedrov, D.; Ayyagari, C.; Smith, G. D. *J. Chem. Theory Comput.* **2006**, *2*, 598.
(2) Cudney, B.; Patel, S.; Weisgraber, K.; Newhouse, Y. *Acta Crystallogr. D* **1994**, *50*, 414.
(3) Mcpherson, A. *J. Cryst. Growth* **1991**, *110*, 1.
(4) Andrade, J. D.; Hlady, V.; Jeon, S. I. *Hydrophilic Polym.* **1996**, *248*, 51.
(5) Poon, W. C. K.; Pirie, A. D.; Haw, M. D.; Pusey, P. N. *Physica A* **1997**, *235*, 110.
(6) Rex, S.; Zuckermann, M. J.; Lafleur, M.; Silvius, J. R. *Biophys. J.* **1998**, *75*, 2900.
(7) Smith, G. D.; Bedrov, D. *Macromolecules* **2002**, *35*, 5712.
(8) Borodin, O.; Bedrov, D.; Smith, G. D. *Macromolecules* **2001**, *34*, 5687.
(9) Tasaki, K. *J. Am. Chem. Soc.* **1996**, *118*, 8459.
(10) Liu, H. Y.; Müller-Plathe, F.; van Gunsteren, W. F. *J. Chem. Phys.* **1995**, *102*, 1722.
(11) Engkvist, O.; Astrand, P. O.; Karlstrom, G. *J. Phys. Chem.* **1996**, *100*, 6950.
(12) Williams, D. J.; Hall, K. B. *J. Phys. Chem.* **1996**, *100*, 8224.
(13) Smith, G. D.; Borodin, O.; Bedrov, D. *J. Comput. Chem.* **2002**, *23*, 1480.
(14) Anderson, P. M.; Wilson, M. R. *Mol. Phys.* **2005**, *103*, 89.
(15) Smith, G. D.; Jaffe, R. L.; Yoon, D. Y. *J. Phys. Chem.* **1993**, *97*, 12752.
(16) Müller-Plathe, F.; van Gunsteren, W. F. *Macromolecules* **1994**, *27*, 6040.
(17) Bedrov, D.; Pekny, M.; Smith, G. D. *J. Phys. Chem. B* **1998**, *102*, 996.
(18) Stubbs, J. M.; Potoff, J. J.; Siepmann, J. I. *J. Phys. Chem. B* **2004**, *108*, 17596.
(19) Van der Spoel, D.; Lindahl, E.; Hess, B.; Groenhof, G.; Mark, A. E.; Berendsen, H. J. C. *J. Comput. Chem.* **2005**, *26*, 1701.
(20) Lindahl, E.; Hess, B.; van der Spoel, D. *J. Mol. Modeling* **2001**, *7*, 306.
(21) Nose, S. *Mol. Phys.* **1984**, *52*, 255.
(22) Hoover, W. G. *Phys. Rev. A* **1985**, *31*, 1695.
(23) Parrinello, M.; Rahman, A. *J. Appl. Phys.* **1981**, *52*, 7182.
(24) Nose, S.; Klein, M. L. *Mol. Phys.* **1983**, *50*, 1055.
(25) Essmann, U.; Perera, L.; Berkowitz, M. L.; Darden, T.; Lee, H.; Pedersen, L. G. *J. Chem. Phys.* **1995**, *103*, 8577.
(26) Ryckaert, J. P.; Ciccotti, G.; Berendsen, H. J. C. *J. Comput. Phys.* **1977**, *23*, 327.
(27) Horn, H. W.; Swope, W. C.; Pitera, J. W.; Madura, J. D.; Dick, T. J.; Hura, G. L.; Head-Gordon, T. *J. Chem. Phys.* **2004**, *120*, 9665.
(28) Allen, M. P.; Tildesley, D. J. *Computer Simulations of Liquids*; Oxford Science Publications: Oxford, 1987.
(29) Jorgensen, W. L. *J. Phys. Chem.* **1986**, *90*, 1276.
(30) Bedrov, D.; Borodin, O.; Smith, G. D. *J. Phys. Chem. B* **1998**, *102*, 5683.
(31) Bedrov, D.; Borodin, O.; Smith, G. D.; Trouw, F.; Mayne, C. *J. Phys. Chem. B* **2000**, *104*, 5151.
(32) Wick, C. D.; Theodorou, D. N. *Macromolecules* **2004**, *37*, 7026.
(33) Goutev, N.; Ohno, K.; Matsuura, H. *J. Phys. Chem. A* **2000**, *104*, 9226.
(34) Anderson, P. M.; Wilson, M. R. *J. Chem. Phys.* **2004**, *121*, 8503.
(35) Bedrov, D.; Smith, G. D. *J. Chem. Phys.* **1998**, *109*, 8118.
(36) Boulougouris, G. C.; Economou, I. G.; Theodorou, D. N. *J. Phys. Chem. B* **1998**, *102*, 1029.
(37) Tritopoulou, E. A.; Economou, I. G. *Fluid Phase Equilib.* **2006**, *248*, 134.
(38) Krouskop, P. E.; Madura, J. D.; Paschek, D.; Krukau, A. *J. Chem. Phys.* **2006**, *124*.

(39) Mills, R. *J. Phys. Chem.* **1973**, *77*, 685.
(40) Oreilly, D. E.; Peterson, E. M. *J. Chem. Phys.* **1971**, *55*, 2155.
(41) Murday, J. S.; Cotts, R. M. *J. Chem. Phys.* **1970**, *53*, 4724.
(42) Holz, M.; Heil, S. R.; Sacco, A. *Phys. Chem. Chem. Phys.* **2000**, *2*, 4740.
(43) de Gennes, P. G. *Introduction to Polymer Dynamics*; Cambridge University Press: New York, 1990.
(44) Strobl, G. R. *The Physics of Polymers: Concepts for Understanding Their Structures and Behavior*; Springer: Berlin, 1996.
(45) Kawaguchi, S.; Imai, G.; Suzuki, J.; Miyahara, A.; Kitano, T. *Polymer* **1997**, *38*, 2885.
(46) Devanand, K.; Selser, J. C. *Macromolecules* **1991**, *24*, 5943.
(47) Flyvbjerg, H.; Petersen, H. G. *J. Chem. Phys.* **1989**, *91*, 461.
(48) Reith, D.; Müller, B.; Müller-Plathe, F.; Wiegand, S. *J. Chem. Phys.* **2002**, *116*, 9100.
(49) Smith, G. D.; Bedrov, D.; Borodin, O. *J. Am. Chem. Soc.* **2000**, *122*, 9548.
(50) Shimada, K.; Kato, H.; Saito, T.; Matsuyama, S.; Kinugasa, S. *J. Chem. Phys.* **2005**, *122*.
(51) Jorgensen, W. L.; Maxwell, D. S.; TiradoRives, J. *J. Am. Chem. Soc.* **1996**, *118*, 11225.
(52) Das, B.; Roy, M. N.; Hazra, D. K. *Indian J. Chem. Technol*. **1994**, *1*, 93.
(53) Wallace, W. J.; Mathews, A. L. *J. Chem. Eng. Data* **1964**, *9*, 267.
(54) Henni, A.; Tontiwachwuthikul, P.; Chakma, A. *J. Chem. Eng. Data* **2004**, *49*, 1778.